Rock and Soil Mechanics 2024 45(3): 857−866 ISSN 1000−7598
https: //doi.org/10.16285/j.rsm.2023.5351 journal homepage: rocksoilmech.whrsm.ac.cn

Rock strength identification while drilling based on percussive rotary drilling

LIU Yong-bin[1], ZHANG Xiao-ping[1], LI Xin-fang[1], LI De-hong[2], CHEN Guang-jun[3], LIU Xiao-bo[4], XIONG Xue-fei[4], YANG Lang[4], LI Yu-sheng[5]

1. School of Civil Engineering, Wuhan University, Wuhan, Hubei 430072, China
2. China Railway Construction Kunlun Investment Group Co., Ltd., Chengdu, Sichuan 610040, China
3. Sichuan Shu Dao Expressway Group Co., Ltd., Chengdu, Sichuan 610094, China
4. Sichuan Chuanqian Expressway Co., Ltd., Chengdu, Sichuan 646500, China
5. Jiangxi Provincial Communications Investment Group Co., Ltd., Nanchang, Jiangxi 330025, China

Abstract: During tunnel excavation, the digital drilling process monitoring (DPM) system can quickly obtain rock strength parameters in real time, and guide on-site excavation and support operations in a timely manner. In order to obtain the surrounding rock strength in front of the tunnel face in real time, this study carried out the in situ digital drilling tests based on the digital drilling process monitoring (DPM) system mounted on the pneumatic percussion rotary drilling rig. Through the real-time monitoring, recording and analysis of the drilling parameters such as thrust pressure, rotation pressure, percussion pressure and drill rod displacement in the whole drilling process, the characteristics of the drilling parameters in different drilling processes are obtained. On this basis, each drilling process is identified, and the drilling parameters of the pure drilling process are separated by using the DPM time series analysis method. The results show that the drilling depth of the pure drilling process changes linearly with the drilling time. The variation of working pressure of the drilling rig with the drilling time is relatively constant, and it has limited influence on the rate of penetration in different rate-of-penetration sections. Meanwhile, the rate of penetration decreases with the increase in rock strength, and an exponential relationship model between rock strength and rate of penetration is established to guide engineering practice.

Keywords: percussive rotary drilling; drilling process monitoring; drilling parameters; saturated uniaxial compressive strength

1 Introduction

The physico-mechanical parameters of rock are essential for classifying rock mass quality and designing excavation and support systems in underground engineering[1]. The methods commonly used for testing rock physico-mechanical properties include laboratory and in situ testing methods[2−4]. The laboratory testing methods mainly include uniaxial compression test, triaxial compression test, direct shear test, and Brazilian splitting test. These methods require on-site sampling and transportation to the laboratory for testing and analysis. The in situ testing methods mainly include the point load test, in situ stress test, and penetration test, which are more closely aligned with engineering reality than the laboratory testing methods. However, these methods suffer from drawbacks such as operational complexity, prolonged time requirements, high costs, and testing delays. In addition to direct testing methods, there are also indirect testing methods such as sonic test and hydraulic fracturing, which can determine the physico-mechanical properties of rock mass[5−7]. However, these methods still have some shortcomings. For example, the sonic test requires specialized drilling and filling of coupling agents, which makes the detection process complex and time-consuming; hydraulic fracturing involves cumbersome operations and bulky equipment. Hence, there is currently a lack of technologies and methodologies in geotechnical engineering exploration and testing that can rapidly and accurately determine the in situ strength of rock mass.

During tunneling, it is often necessary to verify the results of geophysical exploration through advanced drilling operations[8]. The essence of the drilling process lies in the percussion, shear and torsion exerted by the drill bit on the rock mass. Therefore, drilling data contain rich geological information. Currently, advanced drilling techniques are primarily used for qualitative detection purposes, such as identifying adverse geological conditions like fault zones, caves, and weak interlayers, as well as detecting toxic or harmful gases[9]. It is rarely used for quantitative research on the physico-mechanical properties of rock mass. The abundant geological information embedded within drilling data is often underutilized and discarded.

Digital drilling test technology[10−15] is a method that utilizes specialized digital drilling equipment to control, monitor and analyze various drilling parameters such as drilling speed, rotation rate, torque, percussion force, and

Received: 20 March 2023 Accepted: 23 August 2023
This work was supported by the Science and Technology Research and Development Plan Project of China Railway Construction Kunlun Investment Group Co., Ltd. (KLTZ-KX01-2020-008), Key Research and Development Plan Project of Hubei Province (2021BCA154), the General Fund of National Natural Science Foundation of China (42277160) and the Joint Foundation of Shaanxi Province (2021JLM-48).
First author: LIU Yong-bin, male, born in 2000, Master's degree candidate, focusing on rock mass quality evaluation in underground engineering. E-mail: 1723633433@qq.com
Corresponding author: ZHANG Xiao-ping, male, born in 1982, PhD, Professor, Doctoral supervisor, mainly engaged in scientific research and teaching in underground engineering. E-mail: jxhkzhang@163.com

thrust force during the drilling process. This technology has been widely used in geotechnical engineering for exploration and testing. In the traditional oil, gas and mineral extraction industries, the conventional measurement while drilling (MWD) and logging while drilling (LWD) techniques are commonly employed for data collection during drilling. These techniques acquire the drilling data based on the depth of drilling. For instance, Gui et al.[11] utilized the MWD system to monitor drilling parameters, and identify and divide geological interfaces in geotechnical exploration. In the 1990s, Yue et al.[13] invented the drilling process monitoring (DPM) technique. The main difference between DPM and MWD technology is that DPM collects drilling parameters at regular time intervals rather than based on drilling depth. They applied the DPM technique to in situ geomechanical drilling measurements and concluded that when using the same drilling rig and drill bit to drill holes in the same type of rock, the drilling speed remains constant. Tan et al.[16] mounted the DPM system on a hydraulic rotary drilling rig and investigated the accurate identification of interfaces in intricate weathered granite formations through drilling parameters. Existing research results from the laboratory and on-site digital drilling testing[17–31] also indicate a close correlation between drilling parameters and rock mechanical properties. Teale[17] defined the fracturing-specific energy parameter and conducted the preliminary experiments to study its relationship with uniaxial compressive strength (UCS). Karasawa et al.[18] combined the statistical analysis methods with energy analysis methods to define a rock drillability index and establish a relationship model between drilling parameters and UCS. Zang et al.[19] compared the drilling speeds of similar rocks using different drilling rigs and different rocks with the same drilling rig. They discovered an exponential relationship between the drilling speed and UCS. Huang et al.[20], Kahraman[10], Yaşar et al.[21], Kalantari et al.[22–23] and Wang et al.[24–25] conducted the laboratory or field digital drilling tests to study the relationship between the drilling parameters and UCS. Additionally, He et al.[26], Qiu et al.[27], Liang et al.[28] and Fang et al.[29] utilized the artificial intelligence algorithms based on the MWD technology to predict rock strength and identify rock mass categories. Wang et al.[31] and Li et al.[32] investigated the correlation of the drilling parameters with the rock quality designation (RQD), cohesion, and internal friction angle by employing the MWD technology.

However, most of the research on drilling measurement techniques mentioned above is based on the laboratory drilling experiments conducted with rotary drilling rigs. In practical engineering, percussive rotary drilling rigs are often used for drilling operations. Moreover, the rock-breaking mechanism during percussive rotary drilling differs from that during rotary drilling. Therefore, existing studies on digital drilling have found that it is challenging to accurately simulate the actual drilling process at engineering sites[32]. This study focuses on a specific highway tunnel project where a percussive rotary drilling rig was equipped with a DPM system to conduct the in situ digital drilling experiments. By analyzing the drilling parameters throughout the entire drilling process, characteristic drilling parameter profiles for different drilling processes can be obtained. Based on this analysis, the study separates the time-series curve of the pure drilling process and establishes an exponential relationship model between the drilling speed, percussive rotary drilling, and UCS of saturated rocks.

2 Digital drilling test

2.1 Project overview

The in situ digital drilling test is conducted in a two-way separated highway tunnel. The left lane section spans from chainage Z3K89+901 m to Z3K96+728 m, covering a total distance of 6 827 m with a maximum burial depth of approximately 310 m. Similarly, the right lane extends from chainage K89+910 m to K96+697 m, spanning 6 787 m in total length, with a maximum burial depth of approximately 340 m. The tunnel is located in a structurally eroded area within a low to medium mountainous terrain. The area is characterized by a complex lithology that includes sandstone, shale, limestone and dolomite. The tunnel is located in the central portion of the eastern Yunnan fold belt with complex geological conditions, and it traverses multiple tectonic systems, including the Xiaojiang fault zone, Wanshou Mountain fault zone, and several other fault lines. The overall stability of rocks surrounding the tunnel is moderate.

The section selected for the in situ digital drilling test is located in the inclined shaft at chainage K94 of the tunnel. The surrounding rocks in this section mainly consist of shale with developed joints and fractures. The structural configuration of surrounding rocks is characterized by alternating medium-to-thin layers and medium-to-thick layers, resulting in a blocky fractured pattern. The rock mass is relatively fragmented and contains fissure water (Fig. 1).

Fig. 1 Tunnel face for in situ digital drilling test

2.2 Experimental apparatus and process

2.2.1 Percussive rotary drilling rig

As illustrated in Fig. 2, the fully hydraulic crawler-type drilling rig ZML-120 is used in the in situ digital drilling test. This drilling rig functions as an percussive rotary drilling rig, comprising essential drilling operation components such as a down-the-hole hammer, drill rods, power head, and thrust beam. Its primary technical parameters include an overall mass of approximately 5 000 kg, a drill bit diameter of Φ110 mm, an impactor of 1.0 m in length, drill rod dimensions of Φ89 mm×1.5 m, an output rotation speed of approximately 55 r /min, a maximum output torque of 4 000 N • m, and a maximum feed force of 20 kN.

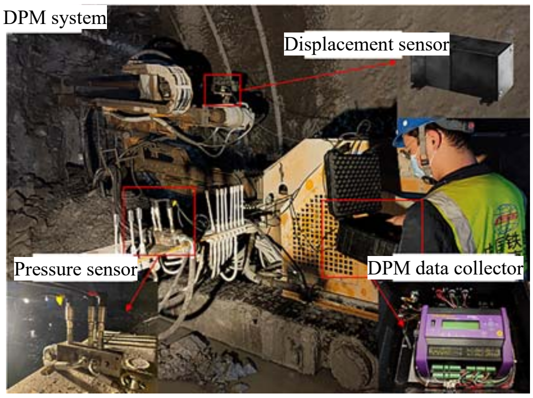

Fig. 2 Drilling process monitoring (DPM) system mounted on pneumatic percussion rotary drilling rig

2.2.2 DPM system

The DPM system is composed of a data acquisition system and a data integration system, as shown in Fig. 2. The data acquisition system primarily consists of sensor units, which include: (1) displacement sensors attached to the power head of the drilling rig are utilized to monitor the displacement of the drill rod and drill bit by tracking the movement of the power head; (2) thrust pressure, rotation pressure, and percussion pressure sensors, all positioned near the power head of the drilling rig, are utilized to monitor the hydraulic pressure applied to the drill rod for thrust, rotation and percussion. The data integration system comprises a DPM data acquisition instrument and a data transmission system, used for transmitting, interpreting and storing electronic or voltage pulse signals. Four types of sensors are used to collect the electronic or voltage pulse signals at a fixed sampling interval of 1 s. The signals are then transmitted to the DPM data acquisition instrument through the data transmission system for interpretation. This allows for the acquisition of the monitored drilling parameters. The operational principle of the DPM system is depicted in Fig. 3.

Before conducting the digital drilling test, the DPM system is mounted on the percussive rotary drilling rig mentioned above. This setup enables real-time monitoring and collection of drilling parameters throughout the entire

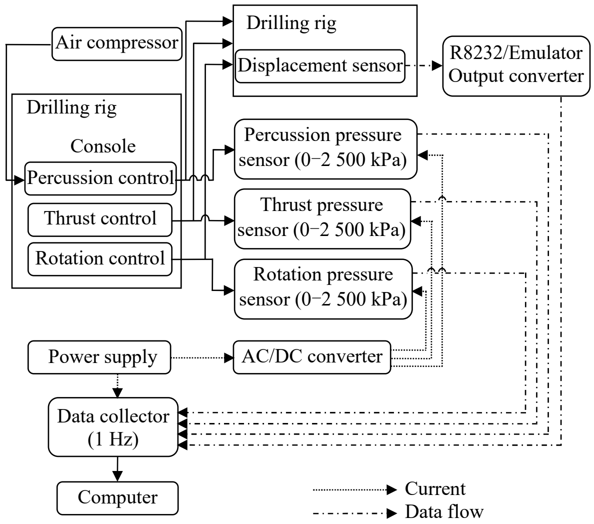

Fig. 3 Working principle of DPM system[13]

drilling process, including drilling time, drill bit displacement, thrust pressure, rotation pressure, and percussion pressure. The in situ digital drilling test is located in the inclined shaft between chainages Z3K94+224.3 m and Z3K94+213.6 m, covering a distance of 10.7 m. The setup for the in situ test is illustrated in Fig. 1.

3 Analysis of drilling monitoring data

3.1 Analysis of raw drilling monitoring data

Figure 4 shows the results obtained from the in situ digital drilling test, which includes a total of five effective drilling parameters: drilling time, drill bit displacement, thrust pressure, rotation pressure, and percussion pressure. The test lasts 8 760 s, from 18 : 50 : 13 to 21 : 16 : 13. It is important to note that the drill bit displacement mentioned here refers to the displacement of the power head of drilling rig.

During the drilling process, the drilling rig undergoes six auxiliary operations: pure penetrating for rock breaking, empty pushing, pulling-back, rod-tightening, rod-untightening, and standby. In actual drilling operations, these auxiliary operations do not occur independently but are often completed in specific combinations to accomplish tasks such as connecting drill rods and addressing rod sticking issue. For instance, the process of connecting drill rods typically involves a sequence of auxiliary operations: pulling-back the drill rods, rod-untightening, standby (adding new drill rods), rod-tightening, and empty pushing. When dealing with a stuck rod, the procedure involves pulling-back the drill rods and gently pushing to clean the hole. In the event of a rig malfunction or downtime, the drilling rig stops working and enters standby mode.

Figure 4(a) shows the displacement-time curve of the drill bit, which exhibits seven distinct rising segments. Each segment corresponds to the drilling process of a single drill rod. The first segment of the rising curve

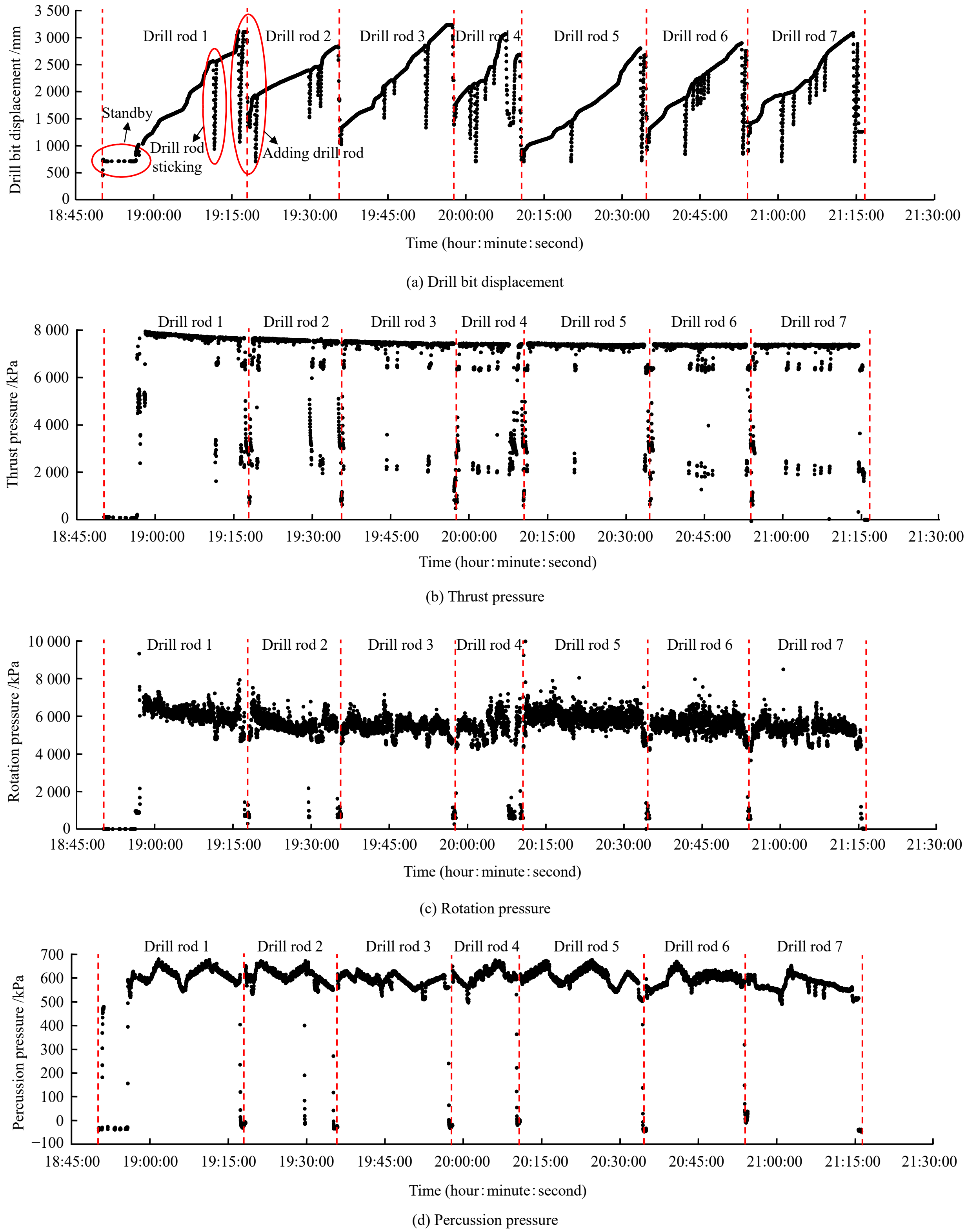

Fig. 4 Changing processes of bit displacement, thrust pressure, rotation pressure and percussion pressure with drilling time

involves the drilling process using the down-the-hole hammer impactor and drill rod, totaling about 2.5 m. The sharp decline in data between adjacent rising segments indicates the process of connecting drill rods. This process involves the rapid pulling-back of the drill rods by the power head of the drilling rig. Upon reaching a specific position during rod pulling-back, the power head reverses rotation to untighten the drill rod, detaching it from the power head. Subsequently, the power head continues to pull back, and a new drill rod is added between the power head and the drill rod. It is then tightened and pushed in to initiate a new drilling process once the drill bit contacts the rock. The process of connecting drill rods is evident in the displacement-time curve by a rapid decrease in drill bit displacement to the starting position, followed by an increase in displacement as a new drilling process begins. The steep drops within each rising segment in Fig. 4(a) are attributed to the reasons such as rod sticking. This issue necessitates a quick pulling-back of the drill rods from the borehole, followed by cleaning the hole, and then empty pushing until the drill bit contacts the rock again to resume drilling. This sequence results in a rapid decrease followed by a rapid increase in drill bit displacement. The horizontal segment within the first rising segment in Fig. 4(a) indicates the standby mode of the drilling rig. During this phase, the drilling rig is not actively drilling, and both the drill rods and the drill bit remain stationary. This is shown as a flat segment in the time-series curve. The slope of the displacement time-series curve in each upward segment indicates the drilling speed, providing an initial evaluation of the drilling efficiency of each drill rod.

During the in situ drilling tests, the drilling rig operators adjusted the rig's operational mode based on different drilling processes. As a result, different drilling processes usually involve varying drilling parameters. Analysis of the actual drilling parameter data presented in Fig. 4 reveals noticeable discrepancies in displacement, thrust pressure, rotation pressure, and percussion pressure between auxiliary operations such as empty pushing, pulling-back, rod-tightening, rod-untightening, standby, and the pure drilling process. Furthermore, the distribution ranges of these parameters also show discrepancies. For example, in Fig. 4(a)−4(d), during the standby process, the displacement, thrust pressure, rotation pressure, and percussion pressure remain constant and close to 0. During the empty pushing process, the displacement increases, while the thrust pressure remains below 7 000 kPa. During the pulling-back process, the displacement decreases, while the thrust pressure remains below 7 000 kPa. During the rod-tightening and rod-untightening processes, the displacement increases and decreases, respectively. The percussion pressure is close to 0, while the thrust pressure and rotation pressure decrease, falling below 7 000 kPa and 4 000 kPa, respectively. During the drilling process, the displacement increases, while the percussion pressure, thrust pressure and rotation pressure are all within normal working conditions, maintaining high-level operations, which are greater than 500, 7 000 kPa and 4 000 kPa, respectively. Therefore, through the analysis of a large amount of drilling data, the characteristics of drilling parameters for different drilling processes are summarized in Table 1. Based on this analysis, various drilling processes of the drilling rig are identified.

The value of E in Table 1 is determined based on the monitored data and represents the maximum displacement per second during drilling by the rig. This value holds physical meaning as it denotes the upper limit of the rig's drilling speed per second. The upper limit of E is determined by excluding the abnormal displacement values, particularly those with larger displacements, given that there is a limit to the normal rock-breaking rate. In this study, the value of E is set to 20.

Table 1 Characteristics of drilling parameters in different drilling processes

Drilling process	Displacement C_i /mm	Percussion pressure P_1 /kPa	Thrust pressure P_2 /kPa	Rotation pressure P_3 /kPa
Empty pushing	$C_{i+1}-C_i>0$	—	<7 000	—
Pulling-back	$C_{i+1}-C_i<0$	—	<7 000	—
Rod-tightening	$C_{i+1}-C_i>0$	≈0	<7 000	<4 000
Rod-untightening	$C_{i+1}-C_i<0$	≈0	<7 000	<4 000
Standby	$C_{i+1}-C_i=0$	≈0	≈0	≈0
Pure drilling	$0<C_{i+1}-C_i<E$	>500	>7 000	>4 000

Note: t_i is the drilling time corresponding to the i-th time interval; and C_i is the corresponding displacement value of the drill bit at time t_i.

During the entire drilling process, the thrusting beam of the drilling rig consistently applies pressure against the tunnel face (Fig. 1). The drilling rig is a crawler-type integrated rig with a total mass of approximately 5 000 kg, which effectively reduces the vibrations in the drilling process for both the rig and the drill rods. Furthermore, due to the high efficiency of percussive rotary drilling in rock breaking, it is observed that during the experimental process, the particle size of the rock chips primarily ranges from 0.5 mm to 5.0 mm, indicating relatively small rock chips. Additionally, the diameter difference between the drill rods and the borehole is 21 mm. Therefore, adjusting the flushing fluid flow rate can promptly discharge the rock chips generated during the drilling process. This helps in reducing the effect of rock chip friction on drilling parameters.

3.2 Analysis of drilling parameters during pure drilling process

As the drill rod length and drilling depth increase, the impacts of drill rod weight and friction against the borehole wall on drilling parameters become more pronounced. This phenomenon creates discrepancies between the monitored data at the power head of drill rig and the actual drilling parameters at the drill bit for rock breaking. These discrepancies primarily manifest in variations in the working pressure of drilling rig. Thus, to accurately determine the true pressure for rock breaking at the drill bit, it is imperative to correct the three types of working pressure of the drilling rig. This correction is based on the changes in working pressure observed when the drill rods rotate freely before and after additional rods are added. This modification can be considered as the impacts of drill rod weight and friction on the effective pressure for rock breaking. The corrected equations are expressed as follows:

$$\Delta w_i = w_i - w_{i-1} \tag{1}$$

$$p_{i\text{-corrected}} = p_{i\text{-measured}} - \Delta w_i \tag{2}$$

where w_i is the working pressure (kPa) when the i-th drill rod is added and rotates freely; Δw_i is the increment of working pressure (kPa) caused by the weight and friction of the i-th drill rod after it is added; $p_{i\text{-measured}}$ is the measured working pressure (kPa) during the drilling process after adding the i-th drill rod; and $p_{i\text{-corrected}}$ is the corrected working pressure (kPa) after mitigating the effects of weight and friction following the addition of the i-th drill rod.

After making the aforementioned correction, and following the characteristics of drilling parameters for various drilling processes (Table 1), appropriate pressure and displacement thresholds are set. Subsequently, the DPM time-series analysis method[13] is utilized to distinguish and exclude the drilling parameters of the auxiliary drilling processes within the entire drilling operation. This procedure facilitates the extraction of essential data related to displacement, thrust pressure, rotation pressure, and percussion pressure during the pure drilling process. Figure 5 illustrates the variation curve of drill bit displacement in relation to pure drilling time, after filtering out the auxiliary DPM data. The slope of this curve reveals the actual drilling speed of the drilling rig. Through the cumulative summation of drill bit displacements for the seven drill rods depicted in Fig. 5, as per Eqs. (3)–(5), the time-series curve illustrating the pure drilling process can be derived (Fig. 6):

$$\Delta x(\Delta t_i) = x(t_i) - x(t_{i-1}) \tag{3}$$

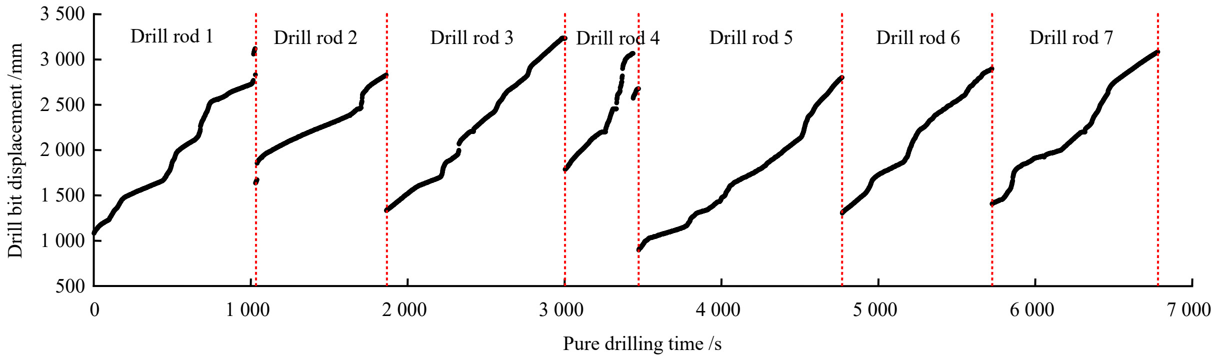

Fig. 5 Changing processes of bit displacement with pure drilling time

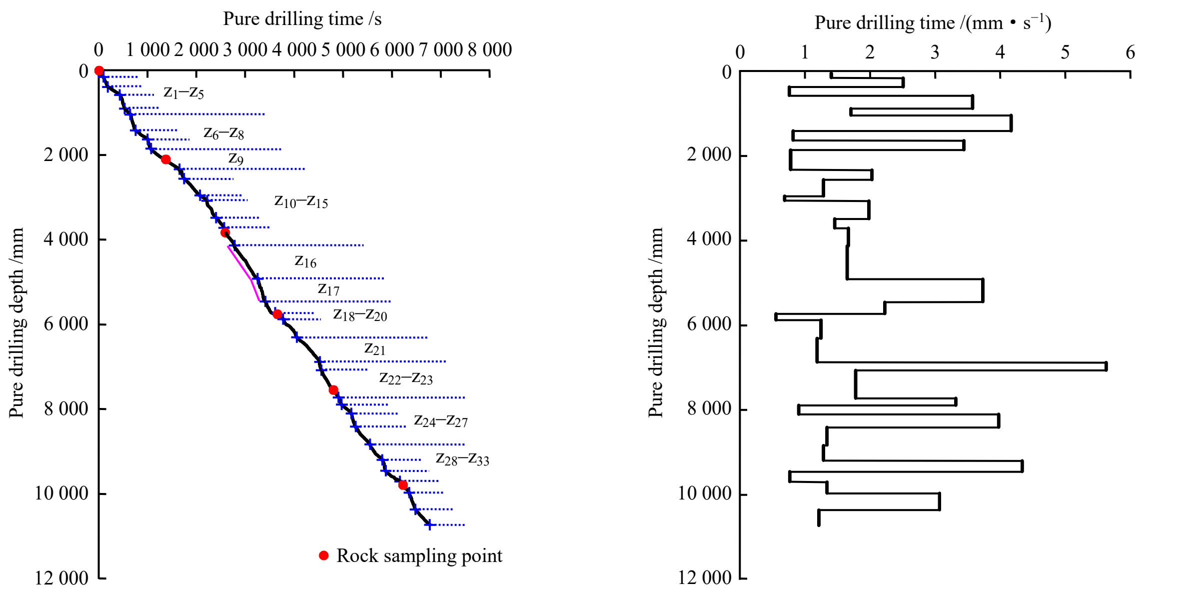

(a) Variation curve of drill bit displacement with pure drilling time (b) Drilling speed with bit advancement curve according to pure drilling time

Fig. 6 Changing processes of pure drilling depth with pure drilling time

$$\Delta t_i = t_i - t_{i-1} = 1\ \text{s} \tag{4}$$

$$s(t_i) = \sum \Delta x(\Delta t_i) \tag{5}$$

where $x(t_i)$ represents the drill bit displacement (mm) at time t_i; $\Delta x(\Delta t_i)$ denotes the drilling depth (mm) during the i-th time interval; and $s(t_i)$ indicates the cumulative drilling depth (mm) at time t_i.

The time-series curve shows 33 relatively distinct linear segments (z_1–z_{33}) (Fig. 6), each displaying a nearly constant drilling speed, illustrating a segmented linear pattern. The length of each linear segment varies from 0.107 m to 0.779 m. By using the least squares method, the linear fitting is performed on each of these segments. The slope of the fitted curve represents the drilling speed of the corresponding segment, indicating the average drilling speed within that segment. The average drilling speed ranges from 0.56 mm /s to 5.63 mm /s, with the coefficient of determination (R^2) for the fitted curve of each linear segment exceeding 0.94. The drilling depth for the pure drilling process illustrated in Fig. 6 measures 10.738 mm, which agrees with the depth manually recorded during the experimental procedure. This further confirms the validity of the distinct drilling parameter characteristics outlined in Table 1 and the DPM time-series methodology. Moreover, the pure drilling operation conducted in this in situ drilling test lasts 6 782 s, resulting in an overall average drilling speed of 1.58 mm /s. The fluctuation in average drilling speed among adjacent linear segments ($\left|(v_{i+1}-v_i)/v_i\right|$, where v_i denotes the average drilling speed of the i-th linear segment) ranges from 3.7% to 373.1%. Such significant differences in average drilling speed between adjacent linear segments verify the correctness of the segment division.

By comparing Fig. 5 with Fig. 6, it is apparent that adding drill rods predominantly occurs within each linear segment, rather than at the transition points of the average drilling speed. Consequently, adding drill rods does not directly cause the changes in the average drilling speed of the linear segments within the time-series curve. This phenomenon could possibly be attributed to the fluctuations in rock strength, elastic modulus, or integrity.

Based on the division of linear segments within the time-series curve of the pure drilling process, the mean values of thrust pressure, rotation pressure, and percussion pressure are calculated for each interval. The respective ranges of distribution for these three types of operational pressures are 7 287−7 864 MPa, 5 342−6 635 MPa and 551−642 MPa. As shown in Fig. 7, the linear correlation coefficients between the operational pressures within each linear segment and the average drilling speed are 0.014, 0.117 and 0.122, respectively. This suggests that the influence of the operational pressure of drilling rig on the variation in average drilling speed is exceedingly limited. Furthermore, the rotation speed of drilling rig is fixed at 55 revolutions per minute, which is a constant parameter. Hence, it can be inferred that the operational parameters of drilling rig do not primarily contribute to the fluctuations in drilling speed within the linear segments of the time-series curve. Instead, they may reflect the alterations in rock strength, elastic modulus, or integrity.

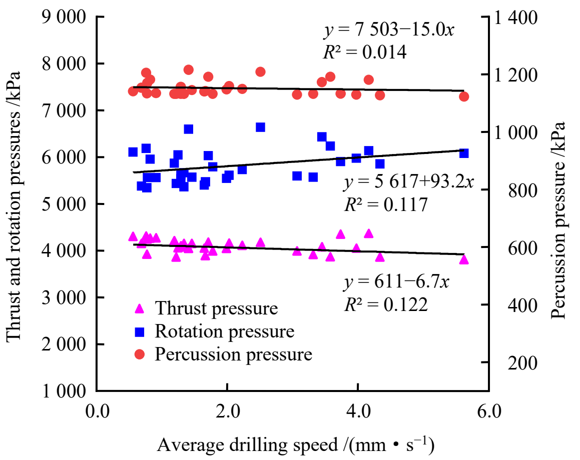

Fig. 7 Relationships of thrust pressure, rotation pressure and percussion pressure with average drilling speed

4 Relationship between drilling speed and rock strength

4.1 Point load strength test of rock

This study uses a pneumatic percussive rotary drilling rig for rock fragmentation. Due to the percussion-rotation technique, acquiring rock cores during the drilling operation is impossible. Hence, to determine rock strength parameters, the intact and undamaged rock specimens are collected from the location beneath the tunnel face at corresponding boreholes after each blasting excavation cycle. Then these specimens are subjected to the point load tests to determine their strengths, without considering the influences of rock mass fractures and other structural parameters induced by blasting disturbances[33−34]. Subsequently, the UCS of saturated rock (R_c) is calculated based on the point load strength index of rock.

The average advance per each blasting excavation cycle in this tunnel is approximately 2.0 m. In the entire digital drilling test section, a total of five blasting excavation cycles are executed. Consequently, six sets of rock samples are collected for rock point load strength analysis, with each set comprising 10−15 rock specimens, totaling 66 specimens. The sampling locations are shown in Fig. 6. All six sets of rock samples are the irregular shale blocks, with dimensions ranging from 42−158 mm in length, 29−124 mm in width, and 36−120 mm in height, as shown in Fig. 8(b). The densities of the tested rock samples range from 1.91 g /cm³ to 2.06 g /cm³.

The digital rock point load tester TC-DHZ1 is used for the rock point load test (Fig. 8). This device is equipped with a liquid crystal display (LCD) screen and possesses a maximum jack output and a rated sensor load capacity of 100 kN. The device meets the testing requirements with a force accuracy of 0.5% and a resolution of 0.01 kN. The method and procedure for the rock point load strength test strictly follow the *Standard for Engineering Classification of Rock Mass* (GB/T 50218—2014)[35]. After the point load test and according to the aforementioned standard, the average point load strength index ($I_{s(50)}$) is calculated for each set of rock samples. The measured $I_{s(50)}$ is then converted into the UCS R_c using the following formula:

$$R_c = 22.82 I_{s(50)}^{0.75} \tag{6}$$

The saturated R_c of the aforementioned rock samples ranges from 21 MPa to 34 MPa, indicating a relatively low strength. These test results are listed in Table 2.

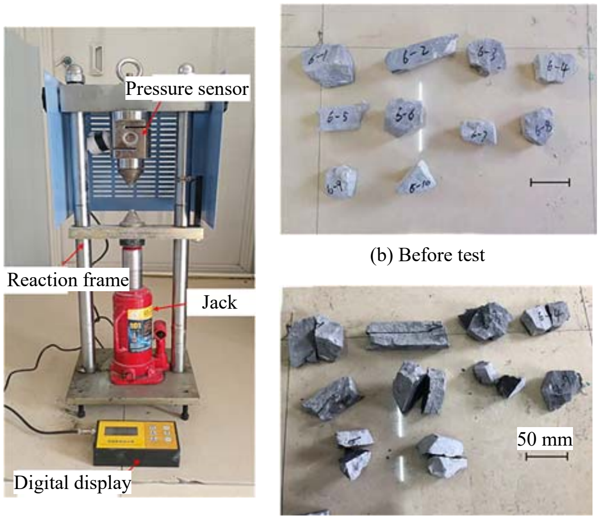

(a) Rock point load test device (b) Before test (c) Before test

Fig. 8 Point load strength test of rock

Table 2 Point load strength test results of rock

Chainage /m	Segment	Rock type	Number of rock samples	$I_{s(50)}$ /MPa	R_c /MPa
Z3K94+224.3	z_1	Shale	15	1.209	26.318
Z3K94+222.2	z_9	Shale	11	1.725	34.351
Z3K94+220.5	z_{15}	Shale	10	0.933	21.666
Z3K94+218.6	z_{18}	Shale	10	1.360	32.643
Z3K94+216.7	z_{23}	Shale	10	1.361	28.761
Z3K94+214.5	z_{31}	Shale	10	1.310	27.950

4.2 Identification of rock strength

Yue et al.[13] found that each constant drilling speed segment represents the uniform resistance properties of rock in that segment, indicative of similar rock mass with their rock strengths generally being close. Therefore, the R_c at each sampling point is taken to represent the UCS of saturated rock within the linear segment where the sampling point is located, as illustrated in Table 3.

Table 3 Average rates of penetration and uniaxial compressive strengths of each section

Segment	Range /mm	v /(mm • s^{-1})	R_c /MPa
z_1	0−159	1.41	26.318
z_9	1 867−2 332	0.78	34.351
z_{15}	3 711−4 130	1.67	21.666
z_{18}	5 455−5 735	0.56	32.643
z_{23}	7 068−7 728	1.61	28.761
z_{31}	9 701−9 967	1.34	27.950

Figure 7 shows that the correlation between the average working pressure and the average drilling speed in each linear segment is low, while the rotation speed of drilling rig remains constant. Thus, it can be inferred that the primary operational parameters of drilling rig, i.e. thrust pressure, rotation pressure, percussion pressure, and rotation speed, exert negligible influence on the variations in drilling speed. Instead, the fluctuations in drilling speed mainly reflect changes in rock strength. Additionally, based on the research findings of Huang et al.[20], the following statistical relationship between drilling speed (v) and the UCS of saturated rock (R_c) may exist:

$$R_c = a\,e^{-bv} \tag{7}$$

where a and b are statistical constants that vary with changes in drill rig type and efficiency, as well as drill bit size and sharpness.

Figure 9 shows a scatter plot depicting the relationship between drilling speed and rock strength. It can be seen that there is an obvious negative correlation between them. This suggests that larger rock strength is associated with slower drilling speed. A power-law relationship model (Eq. (8)) is formulated between the UCS of saturated rock and drilling speed:

$$R_c = -0.841 e^{1.585v} + 35.659 \quad (R^2 = 0.76) \tag{8}$$

To evaluate the accuracy of the model, Eq. (8) is used to calculate the UCS of saturated rock for the six linear segments mentioned earlier. A comparative analysis is conducted between the calculated and measured rock strengths. The results indicate that the deviation between the calculated and measured strengths varies from 2.4% to 15.7%. This indicates that the model demonstrates satisfactory accuracy and can be effectively utilized in engineering applications.

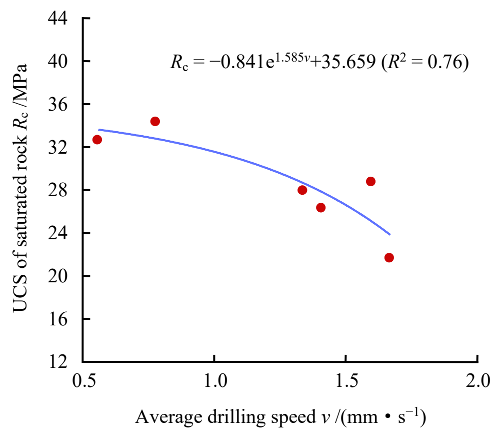

Fig. 9 Relationship between the uniaxial compressive strength of saturated rock and drilling speed

Moreover, given the relatively short length of the linear segments (ranging from 0.107 m to 0.779 m) along the time-series curve shown in Fig. 6, and considering that each blasting excavation cycle covers an approximate distance of 2.0 m, this study only obtains the UCS of saturated rock for six linear segments. Based on this, a relation model between rock strength and drilling speed is established. For the remaining linear segments where rock strength data are not obtained, quantitative estimations of the surrounding rock strength in the tunnel can be derived using the exponential relation model proposed (Eq. (8)). For instance, substituting an average velocity of 1.65 mm /s for z_{16} into Eq. (8) yields the UCS of saturated rock as 24.17 MPa. Similarly, the rock strength of other linear segments can be determined. Furthermore, this relation model can be implemented in later stages of the tunnel project to offer real-time prediction of the surrounding rock strength based on drilling speed. This facilitates guidance for tunnel blasting, excavation, and support operations.

5 Conclusions

(1) Different drilling processes exhibit unique characteristics in drilling parameters, indicating varying distribution ranges. This facilitates the differentiation of diverse drilling processes and the isolation of parameters specific to pure drilling processes.

(2) During the pure drilling process, the drilling depth exhibits segmented linear changes over time, with each linear segment showing relatively stable drilling speed. Each segment of constant drilling speed may represent a uniformly drilling-resistant rock block. Furthermore, abrupt changes in drilling speed between adjacent constant-speed segments are not caused by the addition of new drill rods.

(3) The operational pressure of the percussive rotary drilling rig does not directly cause fluctuations in drilling speed. The impact of variations in drilling speed is limited, suggesting that changes in drilling speed may be attributed to alterations in rock strength, elastic modulus, or integrity.

(4) The drilling speed decreases as rock strength increases during the drilling operation. A model based on the exponential relationship between rock strength and drilling speed derived from percussive rotary drilling has been established.

References

[1] WANG Q, JIANG B, PAN R, et al. Failure mechanism of surrounding rock with high stress and confined concrete support system[J]. International Journal of Rock Mechanics and Mining Sciences, 2018, 102: 89−100.

[2] CAO R, CAO P, LIN H, et al. Mechanical behavior of brittle rock-like specimens with pre-existing fissures under uniaxial loading: experimental studies and particle mechanics approach[J]. Rock Mechanics and Rock Engineering, 2016, 49(3): 763−783.

[3] FERNANDEZ-RODRIGUEZ R, GONZALEZ-NICIEZA C, LOPEZ-GAYARRE F, et al. Characterization of intensely jointed rock masses by means of in situ penetration tests[J]. International Journal of Rock Mechanics and Mining Sciences, 2014, 72: 92−99.

[4] JIA Zhi-xin, WANG Xiao-gang, ZHAO Yu-fei, et al. Application and improvement of rock borehole in-situ test technology[J]. Chinese Journal of Rock Mechanics and Engineering, 2013, 32(6): 1264−1269.

[5] TANG X, XU S, ZHUANG C, et al. Assessing rock brittleness and fracability from radial variation of elastic wave velocities from borehole acoustic logging[J]. Geophysical Prospecting, 2016, 64(4): 958−966.

[6] LI Wen, TAN Zhuo-ying. Prediction of uniaxial compressive strength of rock based on P-wave modulus[J]. Rock and Soil Mechanics, 2016, 37(Suppl.2): 381−387.

[7] LI Hao-ran, YANG Chun-he, LIU Yu-gang, et al. Experimental study of ultrasonic velocity and acoustic emission properties of salt rock under uniaxial compression load[J]. Chinese Journal of Rock Mechanics and Engineering, 2014, 33(10): 2107−2116.

[8] LI Shu-cai, LIU Bin, SUN Huai-feng, et al. State of art and trends of advanced geological prediction in tunnel construction[J]. Chinese Journal of Rock Mechanics and Engineering, 2014, 33(6): 1090−1113.

[9] LI Shu-cai, XUE Yi-guo, ZHANG Qing-song, et al. Key technology study on comprehensive prediction and early-warning of geological hazards during tunnel construction in high risk-karst areas[J]. Chinese Journal of Rock Mechanics and Engineering, 2008(7): 1297−1307.

[10] KAHRAMAN S. Rotary and percussive drilling prediction using regression analysis[J]. International Journal of Rock Mechanics and Mining Sciences, 1999, 36(7): 981−989.

[11] GUI M W, SOGA K, BOLTON M D, et al. Instrumented borehole drilling for subsurface investigation[J]. Journal of Geotechnical and Geoenvironmental Engineering, 2002, 128(4): 283−291.

[12] SONG Ling, LI Ning, LIU Feng-yin. Research on applicable feasibility of rotary penetration technique in harder strata[J]. Rock and Soll Mechanics, 2011, 32(2): 635−640.

[13] YUE Zhong-qi. Drilling process monitoring for refining and upgrading rock mass quality classification methods[J]. Chinese Journal of Rock Mechanics and Engineering, 2014, 33(10): 1977−1996.

[14] WANG X F, ZHANG M S, YUE Z Q. In-situ digital profiling of soil to rock strength from drilling process monitoring of 200 m deep drillhole in loess ground[J]. International Journal of Rock Mechanics and Mining Sciences, 2021, 142: 104739.

[15] WANG Qi, GAO Hong-ke, JIANG Zhen-hua, et al. Development and application of a surrounding rock digital drilling test system of underground engineering[J]. Chinese Journal of Rock Mechanics and Engineering, 2020, 39(2): 301−310.

[16] TAN Zhuo-ying, CAI Mei-feng, YUE Zhong-qi, et al. Interface identification of intricate weathered granite ground investigation in Hong Kong using drilling parameters[J]. Chinese Journal of Rock Mechanics and Engineering, 2006(Suppl.1): 2939−2945.

[17] TEALE R. The concept of specific energy in rock drilling[C]// International Journal of Rock Mechanics and Mining Sciences & Geomechanics Abstracts. Pergamon: [s. n.], 1965.

[18] KARASAWA H, OHNO T, KOSUGI M, et al. Methods to estimate the rock strength and tooth wear while drilling with roller-bits-part 1: milled-tooth bits[J]. Journal of Energy Resources Technology, 2002, 124(3): 125−132.

[19] ZANG Chuan-wei, HUANG Hong-wei, ZHANG Zi-xin. Review on relationship between drilling rate and rock mechanical parameters in a Tunnel[J]. Chinese Journal of Underground Space and Engineering, 2008, 4(3): 415−419.

[20] HUANG S L, WANG Z W. The mechanics of diamond core drilling of rocks[J]. International Journal of Rock Mechanics & Mining Sciences, 1997, 34(3−4): 612.

[21] YAŞAR E, RANJITH P G, VIETE D R. An experimental investigation into the drilling and physico-mechanical properties of a rock-like brittle material[J]. Journal of Petroleum Science and Engineering, 2011, 76(3−4): 185−193.

[22] KALANTARI S, HASHEMOLHOSSEINI H, BAGHBANAN A. Estimating rock strength parameters using drilling data[J]. International Journal of Rock Mechanics and Mining Sciences, 2018, 104: 45−52.

[23] KALANTARI S, BAGHBANAN A, HASHEMALHOSSEINI H. An analytical model for estimating rock strength parameters from small-scale drilling data[J]. Journal of Rock Mechanics and Geotechnical Engineering, 2019, 11(1): 135−145.

[24] WANG Qi, QIN Qian, GAO Song, et al. Relationship between rock drilling parameters and rock uniaxial compressive strength based on energy analysis[J]. Journal of China Coal Society, 2018, 43(5): 1289−1295.

[25] WANG Yu-jie, SHE Lei, ZHAO Yu-fei, et al. Experimental study on measurement of rock strength parameters based on digital drilling technology[J]. Chinese Journal of Geotechnical Engineering, 2020, 42(9): 1669−1678.

[26] HE M M, ZHANG Z, REN J, et al. Deep convolutional neural network for fast determination of the rock strength parameters using drilling data[J]. International Journal of Rock Mechanics and Mining Sciences, 2019, 123: 104084.

[27] QIU Dao-hong, LI Shu-cai, XUE Yi-guo, et al. Advanced prediction of surrounding rock classification based on digital drilling technology and QGA-RBF neural network[J]. Rock and Soil Mechanics, 2014, 35(7): 2013−2018.

[28] LIANG Dong-cai, TANG Hua, WU Zhen-jun, et al. Study on formation recognition based on multi drilling parameters and probability classification[J]. Rock and Soil Mechanics, 2022, 43(4): 1123−1134.

[29] FANG Yu-wei, WU Zhen-jun, SHENG Qian, et al. Intelligent recognition of tunnel stratum based on advanced drilling tests[J]. Rock and Soil Mechanics, 2020, 41(7): 2494−2503.

[30] HE M, ZHANG Z, LI N. Prediction of fracture frequency and RQD for the fractured rock mass using drilling logging data[J]. Bulletin of Engineering Geology and the Environment, 2021, 80(6): 4547−4557.

[31] WANG Qi, QIN Qian, GAO Hong-ke, et al. A testing method for rock c-φ parameter based on digital drilling test technology[J]. Journal of China Coal Society, 2019, 44(3): 916−923.

[32] LI Shu-cai, LI Li-ping, SUN Zi-zheng, et al. Key technology analysis and development trend of the equipment for ultra-long directional drilling and grouting[J]. Rock and Soil Mechanics, 2023, 44(1): 1−30.

[33] WEN L, LUO Z Q, YANG S J, et al. A new method for evaluating the rock mass damage index based on the field point load strength[J]. Royal Society Open Science, 2019, 6(3): 22.

[34] CHEN Jian-xun, CHEN Li-jun, LUO Yan-bin, et al. Conversion relationship between uniaxial compressive strength and point load strength of sandy slate[J]. Journal of Traffic and Transportation Engineering, 2022, 22(4): 148−158.

[35] Ministry of Water Resources of the People's Republic of China. GB/T 50218－2014 Standard for engineering classification of rock mass[S]. Beijing: China Planning Press, 2014.